Journal of Alloys and Compounds 682 (2016) 70–79

Contents lists available at ScienceDirect

Journal of Alloys and Compounds

journal homepage: http://www.elsevier.com/locate/jalcom

Enhanced carbon nanotube dispersion in 3YTZP/SWNTs composites and its effect on room temperature mechanical and electrical properties

A. Gallardo-López [a, *], A. Morales-Rodríguez [a], J. Vega-Padillo [a], R. Poyato [b], A. Muñoz [a], A. Domínguez-Rodríguez [a]

[a] Dpto. de Física de la Materia Condensada, ICMSE, CSIC, Universidad de Sevilla, apdo. 1065, 41080 Sevilla, Spain
[b] ICMSE, CSIC-Univ. de Sevilla, Avda. Américo Vespucio 49, 41092 Sevilla, Spain

ARTICLE INFO

Article history:
Received 18 February 2016
Received in revised form
25 April 2016
Accepted 26 April 2016
Available online 27 April 2016

Keywords:
Ceramics
Composite materials
Nanostructured materials
Mechanical properties
Electrical transport
Scanning electron microscopy, SEM

ABSTRACT

In this work, several modifications of the colloidal processing technique and spark plasma sintering (SPS) to prepare yttria tetragonal zirconia composites (YTZP) with single walled carbon nanotubes (SWNT) have been tested with the aim of eliminating SWNT agglomerates. These modifications include high versus low energy ultrasonic agitation during colloidal processing, lyophilization of the 3YTZP/SWNT slurry and electrical insulation during sintering of the composites. Semi-quantitative microstructural characterization of the carbon nanotube distribution in the sintered composites showed that high energy ultrasonic agitation reduces drastically agglomerate size. Lyophilization of the mixed suspensions avoids SWNT bundle size growth. Combination of both produces an enhanced carbon nanotube network distribution along the grain boundaries (GB) due to the absence of carbon nanotube agglomerates and to a limited SWNT bundle size. This results in an increase of the real SWNT content in the GBs up to nominal SWNT content and therefore an enhanced SWNT efficiency in the composites. The agglomerate-free highly-dispersed composites exhibit a decrease in density together with grain size refinement, a decrease in room temperature hardness, an increase in flexural strength and a most significant increase in room temperature electrical conductivity. Improved SWNT distribution also lowers electrical percolation threshold to a very low level in SWNT ceramic composites, <1 vol% SWNT.

1. Introduction

Fabrication of ceramic/carbon nanotube (CNT) composites has been a special interest research topic over the past decade [1–4], although difficulties in processing have led to controversial results in properties such as hardness or fracture toughness [5–13]. The expected reinforcement effect of the carbon nanotubes in a ceramic matrix, which promoted the study of these composites, has not been unambiguously confirmed. Most studies reporting improvements in fracture toughness have used Vickers indentation method, which has been unanimously refused by the scientific community for these composites since the article by Wang et al. [14]. These authors obtained fracture toughness values for alumina/SWNT composites similar or lower than monolithic alumina by V-SENB (V-single edge notched beam) technique, showing that the extremely high toughness reported for these composites due to the absence of cracks after Vickers indentation was not obtained with other methods. Very recent studies which also use SENB techniques report no reinforcement at all due to carbon nanotubes [15]. The lack of significant reinforcement in carbon nanotube ceramic composites has been attributed to different reasons: densification problems [9,10,16], agglomeration of carbon nanotubes [17–23], damage or defects in the carbon nanotubes [24,25] and poor interfacial bonding [7]. Many steps have been made towards fabrication of pore free and uniformly dispersed carbon nanotube/ceramic composites. To improve CNT dispersion, functionalization of the carbon nanotubes by acid treatment [20,26], colloidal processing [1,3,26–29], heterocoagulation [10,16,29] and charge stabilization techniques [26] have been used. Spark plasma sintering achieve high densification and minimize damage to the CNTs [8,10,30,31] in the composites. In spite of the above mentioned efforts, still a small percentage of carbon nanotubes in ceramic/CNT

* Corresponding author.
E-mail address: angela@us.es (A. Gallardo-López).

http://dx.doi.org/10.1016/j.jallcom.2016.04.262
0925-8388/

composites remain in agglomerates, especially in the case of single walled carbon nanotubes [27,32] due to their high tendency to aggregate via Van der Waals forces and also due to thermodynamic considerations for the particular geometry of the SWNTs compared to the ceramic powder [25,27]. Although recent studies show that these agglomerates are not responsible for the degraded mechanical properties in alumina/SWNT composites [7,33], they are not desirable for several reasons. They introduce heterogeneities in the composites and most important, they decrease SWNT efficiency since when agglomeration occurs the real quantity of SWNT dispersed in the grain boundaries does not coincide with the nominal amount of SWNT introduced in the composite.

Recent works devoted to the study of processing techniques which improve the homogeneity of 3YTZP and alumina composites minimizing SWNT agglomeration [9,23,27,34–36] have shown the importance of an optimal SWNT dispersion in electrical and mechanical properties. Shin et al. [9] used dimethylformamide (DMF) solvent and tip sonication to lower electrical resistivity and increase wear resistance of the more homogeneous composites. Poorteman et al. [27] optimized electrostatic repulsion during colloidal processing and used freeze drying to obtain alumina composites with lower electrical percolation threshold. Poyato et al. [35] lowered electrical percolation threshold of 3YTZP composites and obtained a significant increase in electrical conductivity using a similar colloidal processing with tip sonication. Hu et al. [34] grew CNT in situ on fiber surfaces to prevent agglomeration and coated CNTs with pyrolytic carbon to optimize interfacial bonding of CNT to a SiC ceramic matrix improving its mechanical properties. Zhou et al. [23] used a heterocoagulation pretreatment which improved fracture toughness and flexural strength of the composites. Castillo-Rodríguez et al. [36] reported enhanced plasticity at high temperature of 3YTZP/SWNT composites with improved SWNT dispersion and pointed to interesting microstructural effects of some colloidal processing routines which include the combined used of ultrasonic probe, ball milling and lyophilization. However, the good dispersion obtained for some processing conditions was sometimes obscured by a severe degradation of SWNTs, indicating that processing still needs to be optimized. Further damage to the CNTs can also take place during sintering, due to local heating of the CNTs so electrical isolation has been proposed to minimize it [37].

Most authors report that high CNT content ceramic composites exhibit lower values of hardness, toughness or flexural strength than lower CNT content composites or even than the ceramic matrix [7,10,14–16,18,31,33,38–42]. Therefore, low content SWNT/3YTZP composites (up to 2.5 vol% SWNT) seem more interesting than high SWNT content for structural applications which require good mechanical properties, since they show mechanical properties similar or even superior to the ceramic matrix and they conduct electricity, the percolation limit reported between 0.4 and 1.5 vol% SWNT [43].

Electrical conductivity of ceramic/SWNT composites is very interesting because the isolating ceramic matrix can reach high conductivity values with an appropriate amount and dispersion of the SWNT phase. Different studies have analyzed the influence of SWNT concentration on the electrical conductivity of 3YTZP/SWNT or MWNT composites [43–46], but to the best of our knowledge, only one [35] has focused on the effect of SWNT dispersion on the electrical behavior, pointing to higher conductivity with enhanced SWNT dispersion.

In this work, we have prepared 3YTZP composites with 1 vol% SWNT using several different colloidal processing routines followed by SPS with the main objective of minimizing agglomeration of the SWNTs. The processing routines include high energy sonication for a better SWNT dispersion during colloidal processing, lyophilization of the slurry to avoid a possible SWNT re-agglomeration during drying and electrical isolation of the composite powder during SPS to reduce local heating of the SWNTs. These routines have been carefully applied to obtain optimal distributed SWNT in the ceramic matrix and full densification of the composites with minimum damage to the SWNTs. The different modifications in the processing routines have been introduced step by step to identify the effect of each one independently on the composite microstructure, hardness and electrical conductivity. The effect of the SWNT distribution and real SWNT percentage in grain boundaries on the room temperature electrical and mechanical properties (hardness and flexural strength) of the composites has been systematically analyzed.

2. Experimental

Composites were sintered from commercial 3YTZP powders from Nanostructured and Amorphous Materials Inc. (Houston, Texas) adding 1 vol% (C—OOH) functionalized SWNTs from Nanolab Inc. (Waltham, Massachusetts). The ceramic powders were in a first place annealed at 1250 °C for 30 min in air to remove additives. Colloidal processing of the powders and SWNT was carried out following a basic charge stabilization technique described elsewhere [26]. In this technique both ceramic powder and SWNT are independently suspended in a basic water solution with a small amount of 30% NH_3 solution to acquire a negative surface charge. A small quantity of powder (~3 g) was prepared for each specimen. Two mixing routines have been used. The first, by means of an ultrasonic bath (240 W) applied for 15 min to the independent basic suspensions and a further 15 min to the mixed ceramic powder-SWNT suspension [7]. The second one, by means of a higher power ultrasonic probe (~750 W) (Model KT-600, Kontes Inc. Vineland, NJ) at 20 kHz and 95% amplitude applied for 5 min to the SWNT suspension during 3 cycles, and a further 5 min to the mixed suspension, refrigerating between cycles [35]. The application time of ultrasonic agitation to the suspensions (30 min total with ultrasonic bath and 20 min total with ultrasonic probe) has been lowered considerably with respect to previous works [36] to economize energy and minimize damage to the SWNTs.

Drying of the composite powders has also been carried out by two routes, the first one using a hot plate at 80 °C with continuous stirring; the second one by lyophilization at −80 °C using a Cryodos 80 lyophilizer with nylon filters to avoid powder loss during the process. The composite slurry was immediately frozen after ultrasonic mixing by immersion in liquid nitrogen.

Composite powders were sintered with spark plasma sintering technique (SPS), using a Dr Sinter 1050 Sumitomo Coal Mining Co. This technique is most suitable for ceramic/SWNT composites since sintering temperatures and times are smaller than for conventional methods, thus minimizing damage to the SWNTs and also minimizing grain growth. The powders were introduced in a 15 mm inner diameter conductive graphite die coated with graphite paper and with graphite rods to exert a uniaxial stress during the process. Heating of the powders was achieved by Joule effect when electric current passed through the experimental arrangement. Since the current could also pass through the conductive nanotubes in the composite powder, electrically insulating boron nitride (BN) platelets were placed between the rods and the powders in some samples to assess a possible overheating and damage of the SWNTs when these insulators were not used. All composites were sintered at 1250 °C for 5 min under 75 MPa with 200 °C/min heating and 50 °C/min cooling ramps.

The different processing and sintering routines combining the alternative above mentioned steps (ultrasonic bath or probe; hot plate drying or lyophilization; SPS sintering with or without BN insulation) are summarized in Table 1. Composites are denoted C1, C2 … to C5, where C1 corresponds to the more basic approach and

Table 1
Processing routines followed in this study.

Composite reference	Dispersion method		Composite slurry drying		Isolation during SPS	
	Ultrasonic bath	Ultrasonic probe	Hot plate & stirring	Lyophilization	No electric isolation	BN platelets
C1	x		x		x	
C2		v	x		x	
C3	x			v	x	
C4		v		v	x	
C5		v		v		v

X: simpler processing routine step.
V: modified processing routine step.

C5 to the more refined one.

Density of the sintered composites was measured by the Archimedes method using distilled water as immersion medium. Theoretical density of the composites $\rho = 6.04$ g cm^{-3} was calculated using the rule of the mixtures, considering $\rho = 6.1$ g cm^{-3} for 3YTZP and $\rho = 0.14$ g cm^{-3} for SWNT. Agglomerate and grain size characterization was carried out by scanning electron microscopy (SEM, JEOL 6460LV) and high resolution SEM (HRSEM, Hitachi S5200) respectively on composites polished up to 1 μm diamond paste (CITIUS facilities, University of Seville). To reveal grain boundaries -for estimation of grain size-, polished samples were further annealed in air at 1150 °C for 15 min. The equivalent planar diameter $d = 2\ (\text{area}/\pi)^{1/2}$ was used as size parameter both for 3YTZP grains and for SWNT agglomerates, using a number of grains and agglomerates not less than 200. The direct analysis of the agglomerates has been carried out on 3×2 mm^2 cross sections and top surfaces to scan a sufficiently large area of the sintered samples. The maximum axial dimension and the aspect ratio of the SWNT agglomerates have also been estimated due to their characteristic elongated shape.

To evaluate the presence of SWNTs, their structural integrity and the presence of other carbon allotropes after sintering, Raman vibrational spectroscopy was performed on fractured surfaces of all composites, taking six to eight spectra from each specimen (Raman Horiba Jobin LabRaman HR800 with Labsec 5.25.15 data acquisition software). The source was a green He–Ne laser (532.1 nm) of 20 mW power. Diffraction grid consisted of 600 lines per mm and the 100× objective had a confocal aperture of 100 μm. This spectroscopy was carried out in facilities belonging to the Instituto de Ciencia de Materiales de Sevilla (ICMSE).

X-Ray diffraction performed on plane surfaces of the composites was used to evaluate the presence of different phases. An X-Ray diffractometer D8 Advance A25 (Bruker Co.) from CITIUS facilities was used.

Vickers microhardness was evaluated on polished top surface and cross section of the specimens, to account for a possible influence of the uniaxial stress applied during sintering. A Struers Duramin microindenter was used, with loads of 1.96 N during 15 s.

Flexural strength was measured as the maximum stress before breakdown, σ_{max}, in $15 \times 2 \times 1$ mm^3 bars, the surface under tension polished to 1 μm, using a prototype three point bending test arrangement described elsewhere [33], specially designed for the small specimens' size. Correlation with the maximum applied load, F, is given by:

$$\sigma_{max} = \frac{3L}{2h^2w}F$$

where L is the span; h and w are respectively height and width of the sample.

Electrical conductivity of the composites at room temperature was estimated by impedance spectroscopy, using an Agilent 4294A analyzer which operated from 100 to 2×10^6 Hz. Parallelepipedic $15 \times 2 \times 1$ mm^3 bars were cut and colloidal silver paste was applied on two parallel faces. Electrodes were fired at 600 °C for 30 min in Ar flow. The obtained impedance data was analyzed using an equivalent circuit model by means of Z-view software.

3. Results and discussion

3.1. Microstructure

The differences in the experimental routines used for colloidal processing of the five SWNT/3YTZP composites in this study (see Table 1) have a remarkable influence in the microstructure of the sintered bodies.

Information about SWNT agglomeration and distribution into the ceramic matrix can be extracted directly or indirectly from the different characterization methods used (microstructural, mechanical and electrical). Results from microstructural characterization by BSE (backscattered electrons in SEM) carried out on polished cross sections of the composites have been used as the more direct method to quantify the SWNT dispersion (Fig. 1). The presence and distribution of SWNTs and agglomerates can be clearly visualized and measured more reliably than with optical microscopy because of the high contrast due to the average atomic number difference between the ceramic 3YTZP matrix and the light C of SWNT. Grain boundaries in Fig. 1 are visible because of the presence of dark SWNT bundles in them, giving a picture of how the SWNT are distributed. It is most remarkable that only in C1 and C3 some large agglomerates can be observed, while composites which have been processed with high energy ultrasonic tip do not show any large SWNT agglomerates. In C2, C4 and C5 all SWNT appear located at GBs, and are especially visible in C5 (with electrical insulation during SPS). The effect of agglomeration is the coexistence of agglomerates and free-agglomerate areas depleted in SWNTs. This can also be seen in SEM micrographs of fracture surfaces in composites in Fig. 2. C4 and C5 show SWNTs (mainly bundles) in most ceramic grain boundaries, while in C1, some SWNT are in agglomerates and less in grain boundaries. Most SWNT agglomerates appear elongated in the perpendicular direction to the sintering compression axis, as it has been previously reported elsewhere [40], which makes them easier to identify. The aspect ratio has been estimated in ~5 (see Table 2). This elongation of SWNT agglomerates can influence hardness, producing anisotropy in its values when measured in the top surfaces or in cross sections of the sintered composites [40].

The direct analysis of the agglomerates has been carried out considering as agglomerates only groups or bundles of SWNT larger than 2 μm in length (typically corresponding to d ~ 1–1.5 μm equivalent planar diameter). The reason for this choice is that, in cross sections, most agglomerates larger than mentioned exhibit their characteristic elongated shape, while "smaller agglomerates", with size comparable to the ceramic grains, exhibit a rounded

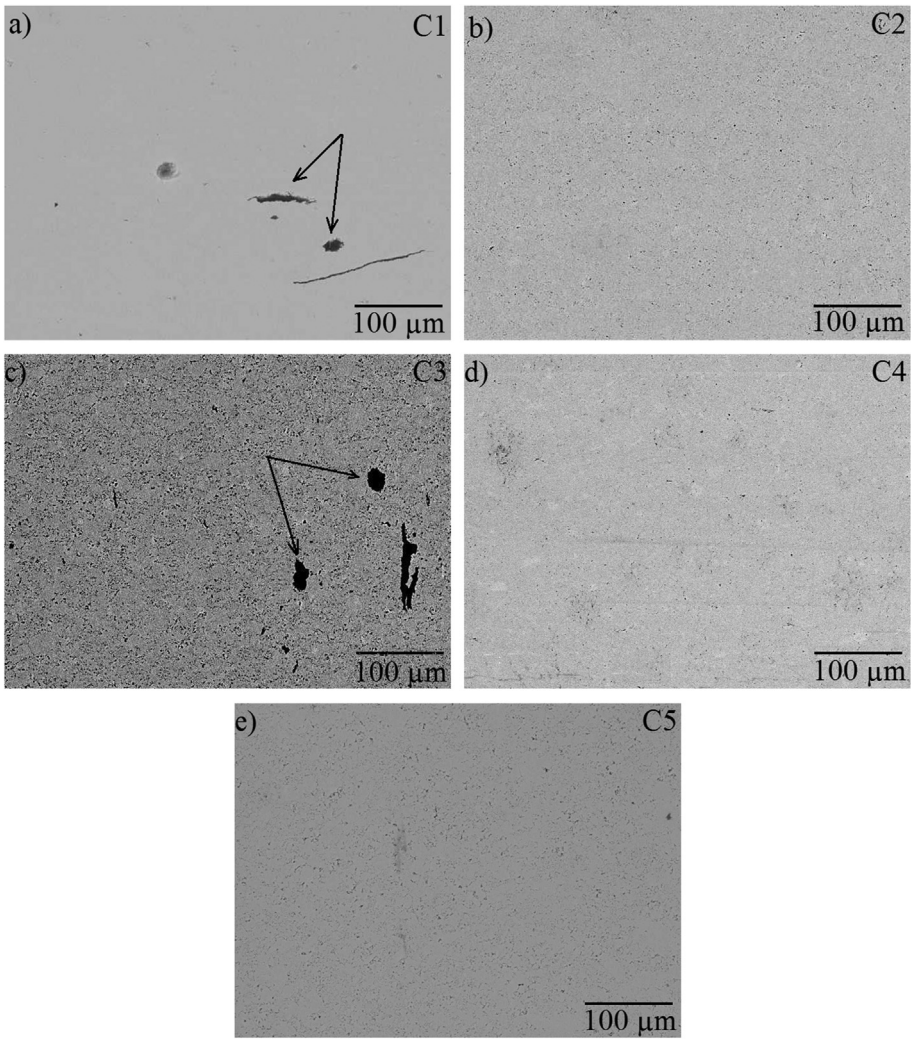

Fig. 1. Low magnification backscattered electron scanning (BSE) images from the indicated composites cross sections, showing dark SWNT in the GBs and some large agglomerates (arrowed). a), b), c), d), and e) correspond to C1, C2, C3, C4 and C5 composites respectively.

shape. These smaller rounded shapes in our 2D images correspond actually to cross sections of bundles whose major axes lie in planes different from the analyzed specimen cross section. Including these "smaller agglomerates" in the analysis would distort the statistics of characterization parameters such as size and aspect ratio, and would also obscure the observations of the much more typical larger elongated agglomerates. Besides, SWNTs are hardly ever found isolated, but in bundles of variable size. Therefore, the frontier between a big bundle and a small agglomerate is not so clear for sizes under ~1–1.5 μm.

Our results from direct agglomerate BSE analysis (presented in Table 2) indicate that the surface agglomerate density is apparently very low for all the composites. The highest value is 0.5%, found in C3, similar to C1 (0.3%) which both used low energy ultrasonic agitation and no electrical insulation during SPS. This value is also similar to the same composition with alumina matrix processed with the same conditions [40]. However, taking into account that the total SWNT content was 1 vol%, and using the Delesse principle to extrapolate volumetric to surface concentrations, these would mean that half the total SWNT of the composite C3 is in agglomerates while the other half is distributed in the grain boundaries.

The use of an ultrasonic probe during processing (composites C2, C4 and C5) lowers this agglomerate surface density in an order of magnitude (0.02%), so now only 2% of the total SWNT content of the composite is agglomerated while the remaining 98% is well distributed in the grain boundaries (see Fig. 1 and Table 2). This is a huge improvement in the dispersion of SWNTs, as it can be also visualized in Fig. 2. The ultrasonic probe is therefore very successful in eliminating agglomerates. Another microstructural direct effect of the use of the ultrasonic probe is the smaller agglomerate size (X_{max}), (half width along the major axis) although a statistical analysis cannot be carried out due to the negligible quantity of agglomerates found in these composites. In view of these results, the effect of the ultrasonic probe during processing versus lower energy (ultrasonic bath) agitation is double: most important, removing agglomerates almost totally and a secondary effect of reduction in size of the rare remaining agglomerates (40–50%).

Lyophilization of the composite powder suspensions, however, seems not to have a remarkable influence in reducing agglomerates versus drying on a hot plate, since C1 and C3 composites have the same order of magnitude of agglomerate surface density. This means that significant re-agglomeration of the SWNTs does not occur during hot plate drying of the slurry.

Density drop and grain size refinement are also microstructural effects of the homogeneous SWNT dispersion into the ceramic matrix, usually linked to an increased nominal CNT content in the

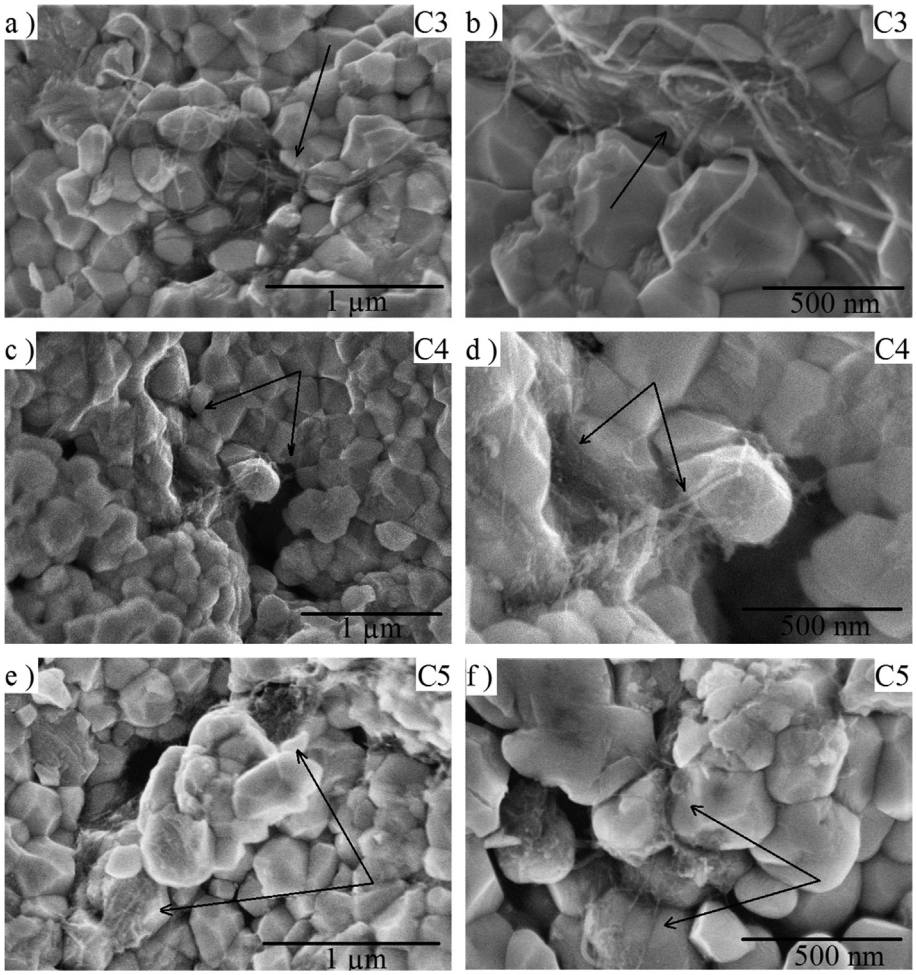

Fig. 2. Fracture surfaces of composites C3, C4, and C5, showing ceramic 3YTZP grains and SWNTs (arrowed) at different magnifications.

Table 2
Experimental relative densities of the composites, ceramic grain size, surface density of SWNT agglomerates, SWNT agglomerates' size, maximum axial dimension and aspect ratio.

Composite reference	ρ_{rel} (%)	3YTZP	SWNT agglomerates			
		<d>±sd (nm)	ρ_{agglom} (%)	<d>±sd (μm)	X_{max} (μm)	Aspect ratio
C1*	100	230 ± 90	0.30	12 ± 9	30	5.6 ± 5.8
C2*	98	210 ± 90	0.02	_	13	_
C3*	99	220 ± 100	0.50	13 ± 13	30	5.1 ± 3.9
C4*	98	190 ± 90	0.07	_	15	_
C5*	97	190 ± 80	0.02	_	23	_

(*) Starred compounds present a negligible amount of agglomerates (only one or two maximum) throughout the analyzed cross section (4 × 2 mm^2), so mean values have been excluded because statistical analysis are not valid for these specimens.

composites [9,16,23,47]. Grain size refinement is due to the SWNT role as grain size inhibitors. Therefore, a better and increased distribution of the SWNTs in the ceramic matrix grain boundaries should also result in a decreased densification and a reduced ceramic grain size. Density of the composites actually decreases when the different modifications to the colloidal processing are used, as can be seen in Table 2. Lyophilization of the slurry (C3) results in a very slight density decrease (versus C1), while the use of high energy agitation (C2 and C4) gives a more pronounced density decrease. Both mentioned modifications together with the use of electrical isolation during SPS produce the minimum density, indicating a better SWNT preservation. Fig. 3 shows polished cross sections annealed in air to reveal grain boundaries. In spite of the small density decrease found, samples are highly dense and the few "pores" observed in this micrograph are due to the burning of SWNT bundles. Grain size also detailed in Table 2 for the different composites, indicates again that the ultrasonic probe is more effective in SWNT dispersion than lower energy (ultrasonic bath) agitation of the powders suspensions, since composite C2 which used the probe show a slightly reduced grain size than C1 (9% decrease). Lyophilization of the composite powder suspension (C3) also reduces, but very slightly, grain size versus C1, with hot plate drying of the slurry (4% decrease). The combined used of the two mentioned techniques (high energy tip ultrasonic agitation of the suspensions and lyophilization of the slurry, C4 and C5) is even more effective in reducing grain size because of the enhanced

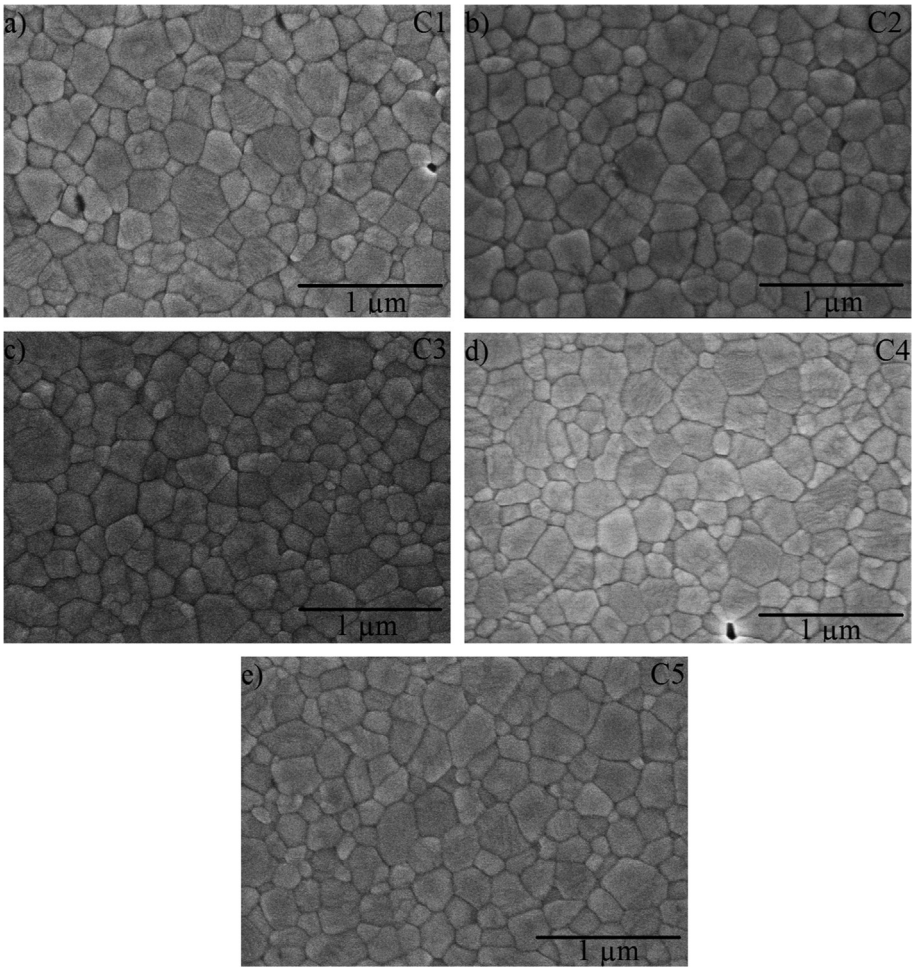

Fig. 3. SEM micrographs of polished cross sections after annealing in air to show 3YTZP grain boundaries. a), b), c), d) and e) correspond to C1, C2, C3, C4 and C5 composites respectively.

SWNT distribution in the sintered composite, producing a 17% decrease in ceramic grain size.

These results indicate that lyophilization does play a role in enhancing SWNT distribution in grain boundaries. It does not reduce large agglomerates, as it has been shown by the quantitative agglomeration analysis, but it can reduce bundle size (which is difficult to quantify in SEM). That is why its effect is more subtle than high energy agitation. If bundle size decreases, there will be more SWNT in grain boundaries, that is, a better SWNT dispersion. During hot plate drying, SWNT do not re-agglomerate in large agglomerates, but they can form thicker bundles. Lyophilization avoids this, maintaining the level of SWNT dispersion achieved with the previous agitation method. This effect of lyophilization could not be detected by agglomerate size analysis, because it does not affect large agglomerates, but density and grain size of the composites indicate it.

The use of an electrical insulator during SPS sintering (C5) does not reduce grain size, but reduces slightly its standard deviation which also points to a more homogeneous SWNT distribution in the grain boundaries and a more homogeneous ceramic grain size distribution due to the absence of local heating. In all composites, grains are fairly equiaxed with an estimated shape factor $F = 0.77 \pm 0.06$. This parameter is not influenced by the sintering routines used.

Another microstructural effect of SWNT dispersion is the presence of monoclinic phase in the tetragonal 3YTZP matrix. Semi-quantitative results from X-Ray diffraction (not shown) indicate the presence of this phase in all composites, with an increase of the two main monoclinic peaks (at 2θ values of 28.2 and 31.4° respectively) which is more significant for composites prepared using ultrasonic probe. This could also be indicative of an increased distribution of the SWNTs in the grain boundaries, since it has been reported in the literature that the transformation of the tetragonal phase to the monoclinic is favored by an increased presence of CNTs in grain boundaries [7,35,48], which may be achieved by increasing nominal SWNT content [7] or by improving SWNT dispersion [35], as in this work. Further work will be carried out to clarify the role of CNTs in the tetragonal to monoclinic transformation.

A presence of C70 fullerene has been detected only when using the ultrasonic probe (in composites C2, C4 and C5). This phase could arise from SWNT collapse [49], may be as a consequence of the high energy supplied by the probe. This fact warns about a possible degradation of SWNTs if too high energies and/or exposure times are used during processing, therefore efforts towards optimization in processing are necessary.

Estimation of I_D/I_G ratio from the Raman spectra (see Fig. 4) of the composites is often used to obtain information about the ratio between defective and non-defective SWNT (Table 3). The G band appears at ~1590 cm^{-1} and is characteristic of SWNT while the D band at ~1350 cm^{-1} is usually associated with crystalline defects in the SWNT. Raman spectra of the SWNT used in this study showed a not negligible D band (I_D/I_G~0.30) which obviously increases I_D/I_G

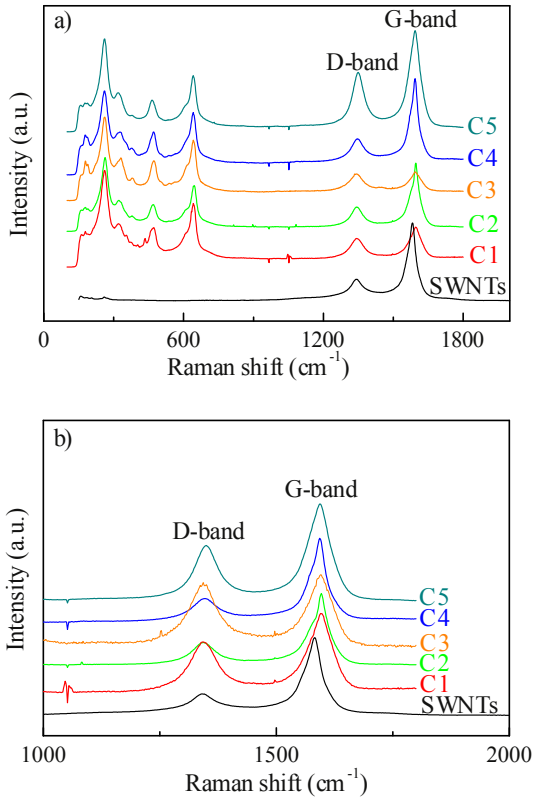

Fig. 4. Raman spectra from the 3YTZP/1 vol% SWNT composites sintered in this study. (a) Spectra normalized to the 3YTZP peaks and (b) area of interest normalized to the G-band for easier comparison.

ratio of the corresponding composites. Smaller I_D/I_G ratios were obtained from composites prepared with similar methods but different SWNTs in previous works [7,43]. Raman spectra from composites C2, C4 and C5, prepared using high energy ultrasonic probe to improve dispersion present systematically a smaller I_D/I_G ratio than composites C1 and C3 processed with lower energy ultrasonic agitation (see values in Table 3), which indicates that the energy and working time of the ultrasonic probe was reasonable and did not damage the SWNT crystallographic integrity. The fact that I_D/I_G ratio in C1 and C3 composites (prepared using low energy ultrasonic bath) is larger than this ratio for composites prepared using high energy ultrasonic probe may seem surprising. It can reach even values >1, as in C3. The occurrence of a D band higher than the G band has already been reported in the literature, for instance in MWNT [25] and very recently in DWNT/3YTZP composites when DWNT content is very high (18 vol%) [42]. The increase of the D band has been explained in the latter case by damage to the DWNTs during SPS due to the mixed ionic-electronic conductivity of the YSZ composite at high temperatures which can induce local heating of the CNTs. The differences observed in the Raman spectra for the composites in this work could be explained as damage related to the presence of CNT agglomerates which would induce local heating during SPS or assuming that agglomerates are considered as defective SWNTs by Raman spectroscopy, increasing D band in composites with more agglomerates. A wide variability of I_D/I_G values has been observed for some composites (C1, C3 and C5), also reported by other authors in DWNT/3YTZP composites and attributed to an uneven damage of the SWNTs [42]. This variability could also be related to the presence of agglomerates, which alter homogeneity of the composites, since composites C2 and C4 which do not show SWNT agglomerates exhibit very similar Raman spectra with a narrow I_D/I_G range (Table 3). The presence of C70 fullerene does not alter significantly the SWNT Raman spectra, and in any case it would not increase D band, according to its own Raman spectra [50].

3.2. Mechanical properties

Hardness of the composites is strongly affected by the processing routines used in this study. Fig. 5 shows the different sizes of Vickers imprints in each composite. The optical micrographs in Fig. 5a illustrate how C2, C4 and C5 which were prepared using high energy ultrasonic tip for agitation during colloidal processing show more SWNTs in GBs and larger Vickers imprints, corresponding to lower hardness (see Table 3); while C1 and C3 with less SWNT distributed in GBs (due to the presence of large agglomerates) present smaller imprints, corresponding to higher hardness values. Imprint sizes are maxima for composite C5 which was prepared using high energy sonication combined with lyophilization of the slurry and electrical insulation during sintering. SWNTs are a softer phase than the ceramic 3YTZP matrix, which can be visualized by the Vickers imprint in Fig. 5b, clearly larger within the SWNT agglomerate area of composite C3. When a sample contains agglomerates large in size (>30 μm), there remain less SWNTs in grain boundaries (equivalent to a smaller nominal SWNT content) so the average hardness value is more similar to the ceramic matrix. Interfacial bonding between 3YTZP ceramic grains and SWNT is not very strong [7], so when SWNTs are mostly located in GBs and more homogeneously distributed, more interconnected, their influence is larger, resulting in a reduced hardness value. Therefore, improving SWNT dispersion decreases hardness because it increases SWNT content in GBs, in an analogous way to the decrease in hardness reported as a consequence of increasing nominal SWNT content in 3YTZP/SWNT composites [7,43]. A larger area of GBs covered by SWNT also facilitates grain boundary sliding at high temperatures, which has been proved by creep tests [36].

Taking hardness values as a measure of the degree of SWNT distribution in grain boundaries (dispersion efficiency), the results obtained (Table 3) tell us that while using a high energy ultrasonic probe improves SWNT distribution (C2, C4, C5), lyophilization of the mixture has an undetectable effect on hardness, so it does not seem to improve SWNT dispersion sufficiently to affect hardness, neither alone (compare C1 and C3) nor combined with probe sonication (compare C2 and C4).

Table 3
Raman I_D/I_G ratio, SWNT content in GBs, Vickers hardness (H_v), flexural strength (σ_F) and electrical conductivity (σ_e) of the composites.

Composite reference	I_D/I_G	I_D/I_G range (min, max)	GB-SWNT content (%)	H_v (GPa)	σ_F (MPa)	σ_e (Sm^{-1})
C1	0.58	(0.26, 0.60)	0.7	13.5 ± 0.6	400 ± 50	Non conductive
C2	0.34	(0.11, 0.37)	1	11.6 ± 0.4	–	0.4 ± 0.2
C3	0.88	(0.19, 1.02)	0.5	13.5 ± 0.9	–	Non conductive
C4	0.36	(0.31, 0.37)	1	11.7 ± 0.7	600 ± 50	2.5 ± 0.5
C5	0.45	(0.40, 0.66)	1	9.6 ± 0.9	–	1.1 ± 0.2

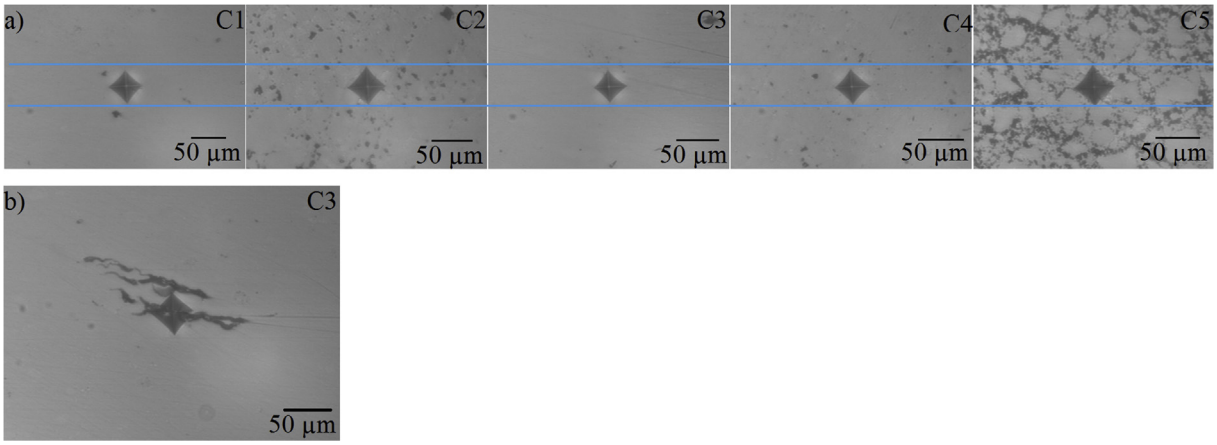

Fig. 5. a) Optical micrographs showing Vickers indentations (1.96 N) on cross sections of the studied composites. b) Non symmetric Vickers imprint on a large SWNT agglomerate in composite C3.

The use of BN as electrical insulator during SPS (C5) also decreases hardness substantially. This fact suggests that electrical insulation is effective in preserving SWNTs. This aspect can also be confirmed by optical microscopy, since polished surfaces of the composites sintered with electrical insulation show a characteristic microstructure different to the rest with more clearly visible SWNTs, as can be seen in Fig. 5.

The results for flexural strength in 3YTZP/SWNT composites sintered in this study are only illustrative, since only few specimens were prepared due to experimental difficulties. The results of flexural strength of composite C4 of this study, $\sigma_F = 600 \pm 50$ MPa, are analogous to the flexural strength for 1 vol% SWNT/Al_2O_3 (in the range 520–610 MPa) [33] (composite tested with the same experimental set up and same specimen dimensions). They are also comparable to the value $\sigma_F = 526 \pm 84$ obtained for 1.2 vol% DWNT/3YTZP [42].

Comparing results for C1 (400 ± 50 MPa) and C4 (600 ± 50 MPa), it could be deduced that flexural strength increases with improved SWNT dispersion. This result can be explained with the same arguments used to analyze flexural strength results from Al_2O_3/SWNT composites [33]. In these alumina composites, with SWNT content ranging from 1 to 3 vol%, flexural strength decreased when SWNT increased. It could seem contradictory that when comparing our results for 3YTZP it appears that now better SWNT dispersed composites do not exhibit the same behavior as composites with higher SWNT content, as it was for hardness. Actually, the reason why flexural strength diminished with SWNT content in alumina composites was attributed to the existence of thicker SWNT bundles on the grain boundaries when SWNT content increased, which diminished grain cohesion. However, better dispersion for a given SWNT amount implies a decrease in both SWNT agglomerate and bundle size in GBs. Since flexural strength is directly correlated to fracture toughness, our results point to a slight increase of fracture toughness when SWNT are better dispersed in the GBs, although this point should be confirmed experimentally.

3.3. Electrical conductivity

The results obtained in this study reflect how the SWNT distribution influences enormously the electrical conductivity of these composites (Table 3), whose composition is just around the percolation threshold. While composites C1 and C3, prepared using low energy sonication during colloidal processing, are isolating, composites C2, C4 and C5, prepared using high energy sonication, are conductive. Therefore, the effect of the use of an ultrasonic probe for dispersion is noticeable, since the composites turn electrically conductive, with conductivity values 0.4, 2.5, and 1.1 Sm^{-1} for C2, C4 and C5 respectively. These values have the same order of magnitude than doped semiconductors or sea water, are higher than reported by some authors with the same carbon nanotube content and comparable to higher (1.7 vol%) CNT content DWNT/3YTZP composites [42]. If we compare C1 and C3 (effect of lyophilization of the composite powder), we cannot see any difference between both composites, since both are isolating. This is due to the fact that in C3 lyophilization is performed on slurry which already has SWNT agglomerates, so the starting agglomerated microstructure is frozen. However, the use of lyophilization in combination with the ultrasonic probe produces a three to six times increase in electrical conductivity (between C2 and C5 or C4). This indicates that lyophilization of a well dispersed composite slurry has a significant effect on the composites electrical properties. The enhanced electrical conductivity is consequence of an improved SWNT distribution with thinner bundles, which cannot be detected by less sensitive microstructural HRSEM observations or hardness measurements (more macroscopical techniques). When SWNT bundle size increases, conductivity decreases in a percolated SWNT network [35,51]. Electrical insulation during sintering does not imply a significant change in electrical conductivity, since the values of C4 and C5 are very similar, slightly higher for C4.

From these results, the correlation between SWNT dispersion and electrical conductivity can be clearly established. We have already obtained that enhancing SWNT dispersion and minimizing agglomeration results in an increased percentage of SWNT in the GBs. It is clear that with small SWNT contents such as used in this study (1 vol%), near the percolation threshold [35,43], a small increase of the SWNTs present in GBs will result in percolating carbon nanotube networks which will make possible electrical conductivity. Thus, measuring electrical conductivity in these materials gives us a very clear and reliable method to asses SWNT distribution in GBs.

On the other hand, the processing techniques used for improving SWNT dispersion have proved to be effective in enhancing electrical conductivity of the composites and in decreasing the percolation threshold of the 3YTZP/SWNT composites below 1 vol%, previously estimated between 1 and 1.5 vol% for composites sintered by a similar processing routine but without high energy ultrasonic probe [35,43].

4. Conclusions

The variety of microstructural, mechanical and electrical characterization techniques used in this study has allowed a thorough assessment of the SWNT distribution in 3YTZP composites with 1 vol% SWNT fabricated using different processing routines.

The use of a high energy ultrasonic probe during colloidal processing of ceramic/SWNT composites affects strongly microstructure of the sintered specimens, with a noticeable reduction of SWNT agglomerates (which are almost negligible in the composites) and therefore increasing the amount of SWNT in the GBs to the nominal content. This enhanced SWNT dispersion results in a decrease of hardness and increase of flexural strength. When used in combination with lyophilization of the composite powder suspensions, distribution of SWNT is further enhanced, since bundle size is constrained (bundle size growth which can take place during conventional hot plate drying is inhibited) and therefore more GBs are covered with SWNTs. This effect is not likely to be detected by SEM or hardness measurements, but it results in grain size refinement, decreased density of the composites and increased electrical conductivity.

Electrical isolation during SPS of the composites preserves SWNTs avoiding local heating during sintering, and produces a more homogeneous grain size distribution.

Improving SWNT distribution in GBs results in conductive composites with a minimum SWNT content, and therefore with the best values of hardness and flexural strength. The improved SWNT dispersion also manages to decrease the electric percolation threshold in these composites to a very low level (<1 vol %).

Acknowledgments

The financial support for this work has been obtained from the Spanish “Ministerio de Economía y Competitividad” (MAT2012-34217) and from the Junta de Andalucía (P12-FQM-1079). XRD and microscopy studies have been performed at CITIUS facilities (Universidad de Sevilla).

References

[1] G.-D. Zhan, J.D. Kuntz, J. Wan, A.K. Mukherjee, Single-wall carbon nanotubes as attractive toughening agents in alumina-based nanocomposites, Nat. Mater 2 (2003) 38–42.
[2] P.J.F. Harris, Carbon nanotube composites, Int. Mater. Rev. 49 (2004) 31–43.
[3] N.P. Padture, Multifunctional composites of ceramics and single-walled carbon nanotubes, Adv. Mater. 21 (2009) 1767–1770, http://dx.doi.org/10.1002/adma.200802270.
[4] J. Cho, A.R. Boccaccini, M.S.P. Shaffer, Ceramic matrix composites containing carbon nanotubes, J. Mater. Sci. 44 (2009) 1934–1951.
[5] J. Cho, F. Inam, M.J. Reece, Z. Chlup, I. Dlouhy, M.S.P. Shaffer, et al., Carbon nanotubes: do they toughen brittle matrices? J. Mater. Sci. 46 (2011) 4770–4779.
[6] J. Sun, L. Gao, M. Iwasa, T. Nakayama, K. Niihara, Failure investigation of carbon nanotube/3Y-TZP nanocomposites, Ceram. Int. 31 (2005) 1131–1134, http://dx.doi.org/10.1016/j.ceramint.2004.11.010.
[7] R. Poyato, A. Gallardo-López, F. Gutiérrez-Mora, A. Morales-Rodríguez, A. Muñoz, A. Domínguez-Rodríguez, Effect of high SWNT content on the room temperature mechanical properties of fully dense 3YTZP/SWNT composites, J. Eur. Ceram. Soc. 34 (2014) 1571–1579. http://dx.doi.org/10.1016/j.jeurceramsoc.2013.12.024.
[8] R.K. Chintapalli, F.G. Marro, B. Milsom, M. Reece, M. Anglada, Processing and characterization of high-density zirconia-carbon nanotube composites, Mater. Sci. Eng. A 549 (2012) 50–59.
[9] J.-H. Shin, S.-H. Hong, Microstructure and mechanical properties of single wall carbon nanotube reinforced yttria stabilized zircona ceramics, Mater. Sci. Eng. A 556 (2012) 382–387, http://dx.doi.org/10.1016/j.msea.2012.07.001.
[10] N. Garmendia, S. Grandjean, J. Chevalier, L.A. Diaz, R. Torrecillas, I. Obieta, Zirconia-multiwall carbon nanotubes dense nano-composites with an unusual balance between crack and ageing resistance, J. Eur. Ceram. Soc. 31 (2011) 1009–1014.
[11] A. Mukhopadhyay, B.T.T. Chu, M.L.H. Green, R.I. Todd, Understanding the mechanical reinforcement of uniformly dispersed multiwalled carbon nanotubes in alumino-borosilicate glass ceramic, Acta Mater 58 (2010) 2685–2697, http://dx.doi.org/10.1016/j.actamat.2010.01.001.
[12] A. Peigney, F.L. Garcia, C. Estournes, A. Weibel, C. Laurent, Toughening and hardening in double-walled carbon nanotube/nanostructured magnesia composites, Carbon N. Y. 48 (2010) 1952–1960, http://dx.doi.org/10.1016/j.carbon.2010.01.063.
[13] L. Shen, Y.-H. Han, C. Xiang, H. Tang, A. Mukherjee, S. Kim, et al., Phase transformation behavior of ZrO2 by addition of carbon nanotubes consolidated by spark plasma sintering, Scr. Mater 69 (2013) 736–739, http://dx.doi.org/10.1016/j.scriptamat.2013.08.015.
[14] X. Wang, N.P. Padture, H. Tanaka, Contact-damage-resistant ceramic/single-wall carbon nanotubes and ceramic/graphite composites, Nat. Mater. 3 (2004) 539–544.
[15] L. Melk, J.J. Roa Rovira, F. García-Marro, M.-L. Antti, B. Milsom, M.J. Reece, et al., Nanoindentation and fracture toughness of nanostructured zirconia/multi-walled carbon nanotube composites, Ceram. Int. 41 (2015) 2453–2461, http://dx.doi.org/10.1016/j.ceramint.2014.10.060.
[16] A. Duszová, J. Dusza, K. Tomášek, G. Blugan, J. Kuebler, Microstructure and properties of carbon nanotube/zirconia composite, J. Eur. Ceram. Soc. 28 (2008) 1023–1027.
[17] J.P. Fan, D.Q. Zhao, M.S. Wu, Z.N. Xu, J. Song, Preparation and microstructure of multi-wall carbon nanotubes-toughened Al2O3 composite, J. Am. Ceram. Soc. 89 (2006) 750–753, http://dx.doi.org/10.1111/j.1551-2916.2005.00774.x.
[18] G. Yamamoto, T. Hashida, Carbon nanotube reinforced alumina composite materials, in: N. Hu (Ed.), Compos. Their Prop., InTech, 2012.
[19] N. Bakhsh, F.A. Khalid, A.S. Hakeem, Synthesis and characterization of pressureless sintered carbon nanotube reinforced alumina nanocomposites, Mater. Sci. Eng. A-Structural Mater. Prop. Microstruct. Process 578 (2013) 422–429, http://dx.doi.org/10.1016/j.msea.2013.04.020.
[20] J. Liu, A.G. Rinzler, H.J. Dai, J.H. Hafner, R.K. Bradley, P.J. Boul, et al., Fullerene pipes, Science 280 (1998) 1253–1256, http://dx.doi.org/10.1126/science.280.5367.1253.
[21] E. Zapata-Solvas, D. Gomez-Garcia, A. Dominguez-Rodriguez, Towards physical properties tailoring of carbon nanotubes-reinforced ceramic matrix composites, J. Eur. Ceram. Soc. 32 (2012) 3001–3020, http://dx.doi.org/10.1016/j.jeurceramsoc.2012.04.018.
[22] M. Estili, Y. Sakka, Recent advances in understanding the reinforcing ability and mechanism of carbon nanotubes in ceramic matrix composites, Sci. Technol. Adv. Mater 15 (2014) 064902, http://dx.doi.org/10.1088/1468-6996/15/6/064902.
[23] J.P. Zhou, Q.M. Gong, K.Y. Yuan, J.J. Wu, Y. fang Chen, C.S. Li, et al., The effects of multiwalled carbon nanotubes on the hot-pressed 3mol% yttria stabilized zirconia ceramics, Mater. Sci. Eng. A 520 (2009) 153–157, http://dx.doi.org/10.1016/j.msea.2009.05.014.
[24] K.E. Thomson, D. Jiang, R.O. Ritchie, A.K. Mukherjee, A preservation study of carbon nanotubes in alumina-based nanocomposites via Raman spectroscopy and nuclear magnetic resonance, Appl. Phys. A-Materials Sci. Process 89 (2007) 651–654, http://dx.doi.org/10.1007/s00339-007-4253-9.
[25] B.T.T. Chu, G. Tobias, C.G. Salzmann, B. Ballesteros, N. Grobert, R.I. Todd, et al., Fabrication of carbon-nanotube-reinforced glass-ceramic nanocomposites by ultrasonic in situ sol-gel processing, J. Mater. Chem. 18 (2008) 5344–5349, http://dx.doi.org/10.1039/b809369e.
[26] R. Poyato, A.L. Vasiliev, N.P. Padture, H. Tanaka, T. Nishimura, Aqueous colloidal processing of single-wall carbon nanotubes and their composites with ceramics, Nanotechnology 17 (2006) 1770–1777, http://dx.doi.org/10.1088/0957-4484/17/6/038.
[27] M. Poorteman, M. Traianidis, G. Bister, F. Cambier, Colloidal processing, hot pressing and characterisation of electroconductive MWCNT-alumina composites with compositions near the percolation threshold, J. Eur. Ceram. Soc. 29 (2009) 669–675.
[28] I. Ahmad, H. Cao, H. Chen, H. Zhao, A. Kennedy, Y.Q. Zhu, Carbon nanotube toughened aluminium oxide nanocomposite, J. Eur. Ceram. Soc. 30 (2010) 865–873.
[29] N. Garmendia, I. Santacruz, R. Moreno, I. Obieta, Slip casting of nanozirconia/MWCNT composites using a heterocoagulation process, J. Eur. Ceram. Soc. 29 (2009) 1939–1945.
[30] A. Datye, K.-H. Wu, G. Gomes, V. Monroy, H.-T. Lin, J. Vleugels, et al., Synthesis, microstructure and mechanical properties of Yttria Stabilized Zirconia (3YTZP) – multi-Walled Nanotube (MWNTs) nanocomposite by direct in-situ growth of MWNTs on Zirconia particles, Compos. Sci. Technol. 70 (2010) 2086–2092, http://dx.doi.org/10.1016/j.compscitech.2010.08.005.
[31] K.E. Thomson, D. Jiang, W. Yao, R.O. Ritchie, A.K. Mukherjee, Characterization and mechanical testing of alumina-based nanocomposites reinforced with niobium and/or carbon nanotubes fabricated by spark plasma sintering, Acta Mater 60 (2012) 622–632. http://dx.doi.org/10.1016/j.actamat.2011.10.002.
[32] O. Tapasztó, L. Tapasztó, M. Markó, F. Kern, R. Gadow, C. Balázsi, Dispersion patterns of graphene and carbon nanotubes in ceramic matrix composites, Chem. Phys. Lett. 511 (2011) 340–343, http://dx.doi.org/10.1016/j.cplett.2011.06.047.
[33] A. Gallardo-López, R. Poyato, A. Morales-Rodríguez, A. Fernández-Serrano, A. Muñoz, A. Domínguez-Rodríguez, Hardness and flexural strength of single-walled carbon nanotube/alumina composites, J. Mater. Sci. 49 (2014) 7116–7123, http://dx.doi.org/10.1007/s10853-014-8419-5.
[34] J. Hu, S. Dong, Q. Feng, M. Zhou, X. Wang, Y. Cheng, Tailoring carbon nanotube/matrix interface to optimize mechanical properties of multiscale composites,

Carbon N. Y. 69 (2014) 621–625, http://dx.doi.org/10.1016/j.carbon.2013.12.005.
[35] R. Poyato, J. Macías-Delgado, A. Gallardo-López, A. Muñoz, A. Domínguez-Rodríguez, Microstructure and impedance spectroscopy of 3YTZP/SWNT ceramic nanocomposites, Ceram. Int. 41 (2015) 12861–12868, http://dx.doi.org/10.1016/j.ceramint.2015.06.123.
[36] M. Castillo-Rodríguez, A. Muñoz, A. Morales-Rodríguez, R. Poyato, A. Gallardo-López, A. Domínguez-Rodríguez, Influence of the processing route on the carbon nanotubes dispersion and creep resistance of 3YTZP/SWCNTs nanocomposites, J. Am. Ceram. Soc. 98 (2015) 645–653, http://dx.doi.org/10.1111/jace.13348.
[37] Q. Huang, D. Jiang, I.A. Ovid'ko, A. Mukherjee, High-current-induced damage on carbon nanotubes: the case during spark plasma sintering, Scr. Mater 63 (2010) 1181–1184, http://dx.doi.org/10.1016/j.scriptamat.2010.08.030.
[38] T. Ukai, T. Sekino, A. Hirvonen, N. Tanaka, T. Kusunose, T. Nakayama, et al., Preparation and electrical properties of carbon nanotubes dispersed zirconia nanocomposites, Key Eng. Mater 317–318 (2006) 661–664.
[39] J. Sun, L. Gao, X.H. Jin, Reinforcement of alumina matrix with multi-walled carbon nanotubes, Ceram. Int. 31 (2005) 893–896, http://dx.doi.org/10.1016/j.ceramint.2004.10.002.
[40] A. Morales–Rodríguez, A. Gallardo–López, A. Fernández–Serrano, R. Poyato, A. Muñoz, A. Domínguez–Rodríguez, Improvement of Vickers hardness measurement on SWNT/Al2O3 composites consolidated by spark plasma sintering, J. Eur. Ceram. Soc. 34 (2014) 3801–3809, http://dx.doi.org/10.1016/j.jeurceramsoc.2014.05.048.
[41] S.W. Kim, W.S. Chung, K.-S. Sohn, C.-Y. Son, S. Lee, Improvement of flexure strength and fracture toughness in alumina matrix composites reinforced with carbon nanotubes, Mater. Sci. Eng. A-Structural Mater. Prop. Microstruct. Process 517 (2009) 293–299, http://dx.doi.org/10.1016/j.msea.2009.04.035.
[42] A. Kasperski, A. Weibel, D. Alkattan, C. Estournès, C. Laurent, A. Peigney, Double-walled carbon nanotube/zirconia composites: preparation by spark plasma sintering, electrical conductivity and mechanical properties, Ceram. Int. 41 (2015) 13731–13738, http://dx.doi.org/10.1016/j.ceramint.2015.08.034.
[43] R. Poyato, J. Macías-Delgado, A. García-Valenzuela, Á. Gallardo-López, A. Morales-Rodríguez, A. Muñoz, et al., Mechanical and electrical properties of low SWNT content 3YTZP composites, J. Eur. Ceram. Soc. 35 (2015) 2351–2359, http://dx.doi.org/10.1016/j.jeurceramsoc.2015.02.022.
[44] S.-L. Shi, J. Liang, Effect of multiwall carbon nanotubes on electrical and dielectric properties of yttria-stabilized zirconia ceramic, J. Am. Ceram. Soc. 89 (2006) 3533–3535, http://dx.doi.org/10.1111/j.1551-2916.2006.01232.x.
[45] S.-L. Shi, J. Liang, Electronic transport properties of multiwall carbon nanotubes/yttria-stabilized zirconia composites, J. Appl. Phys. 101 (2007) 023708, http://dx.doi.org/10.1063/1.2430700.
[46] F.C. Fonseca, R. Muccillo, D.Z. de Florio, L.O. Ladeira, A.S. Ferlauto, Mixed ionic-electronic conductivity in yttria-stabilized zirconia/carbon nanotube composites, Appl. Phys. Lett. 91 (2007) 243107, http://dx.doi.org/10.1063/1.2821373.
[47] J.W. An, D.S. Lim, Effect of carbon nanotube additions on the microstructure of hot-pressed alumina, J. Ceram. Process. Res. 3 (2002) 201–204.
[48] M.H. Bocanegra-Bernal, A. Reyes-Rojas, A. Aguilar-Elguézabal, E. Torres-Moye, J. Echeberria, X-ray diffraction evidence of a phase transformation in zirconia by the presence of graphite and carbon nanotubes in zirconia toughened alumina composites, Int. J. Refract. Met. Hard Mater 35 (2012) 315–318, http://dx.doi.org/10.1016/j.ijrmhm.2012.07.004.
[49] O. Lourie, D.M. Cox, H.D. Wagner, Buckling and collapse of embedded carbon nanotubes, Phys. Rev. Lett. 81 (1998) 1638–1641, http://dx.doi.org/10.1103/PhysRevLett.81.1638.
[50] V. Schettino, M. Pagliai, G. Cardini, The infrared and raman spectra of fullerene C 70. DFT calculations and Correlation with C 60, J. Phys. Chem. A 106 (2002) 1815–1823, http://dx.doi.org/10.1021/jp012680d.
[51] P.N. Nirmalraj, P.E. Lyons, S. De, J.N. Coleman, J.J. Boland, Electrical connectivity in single-walled carbon nanotube networks, Nano Lett. 9 (2009) 3890–3895, http://dx.doi.org/10.1021/nl9020914.